Meso-Cenozoic deformation history of Thailand; insights from calcite U-Pb geochronology

Alexander David Simpson[1,1], Stijn Glorie[1,1], Chris K. Morley[2,2], Nick Roberts[3,3], Jack Gillespie[1,1], and Jack K lee[4,4]

[1]University of Adelaide
[2]PTT Exploration and Production
[3]NERC Isotope Geosciences Laboratory British Geological Survey
[4]Department of Earth Sciences, University of Durham

December 1, 2022

Abstract

U-Pb dating of calcite veins allows direct dating of brittle deformation events. Here, we apply this method to hydrothermal calcite veins in a fold-and-thrust belt and a large scale strike-slip fault zone in central and western Thailand, in an attempt to shed new light on the regional upper crustal deformation history. Calcite U-Pb dates for the Khao Khwang Fold and Thrust Belt (KKFTB) of 221 ± 7 Ma and 216 ± 3 Ma demonstrate that calcite precipitated during tectonic activity associated with stage II of the Indosinian Orogeny (Late Triassic – Early Jurassic). One additional sample from the KKFTB suggests that the Indosinian calcite has locally been overprinted by a Cenozoic fluid event with a different chemistry. For the Three Pagodas Fault Zone (TPFZ), our calcite U-Pb results suggest a complex, protracted history of Cenozoic brittle deformation. Petrographic information combined with contrasting redox-sensitive trace elemental signatures suggest that the vein arrays in the TPFZ precipitated during two distinct events of brittle deformation at 48 and 23 Ma. These dates are interpreted in the context of far-field brittle deformation related to the India-Eurasia collision. The presented calcite U-Pb dates are in excellent agreement with published age constraints on the deformation history of Thailand, demonstrating the utility of the method to decipher complex brittle deformation histories. The paper further illustrates some of the complexities in relation to calcite U-Pb dating and provides suggestions for untangling complex datasets that could be applied to future studies on the deformation history of Thailand and other regions.

Tectonics

Supporting Information for

Meso-Cenozoic deformation history of Thailand; insights from calcite U-Pb geochronology

Alexander Simpson[1], Stijn Glorie[1], Chris K Morley[2], Nick M W Roberts[3], Jack Gillespie[1], Jack K Lee[3,4]

[1]Department of Earth Sciences, The University of Adelaide, SA 5005, Australia

[2]Chiang Mai University, 239 Huaykaew Road, Tumbol Suthep Amphur Muang, Chiang Mai, Thailand

[3]Geochronology and Tracers Facility, British Geological Survey, Keyworth NG12 5GG, UK

[4]Department of Earth Sciences, University of Durham, Science Labs, Durham

Contents of this file

Extended Method Supplementary Figure 1 Supplementary Table 1

Additional Supporting Information (Files uploaded separately)

Supplementary Data file 1 (U-Pb and Trace element data) Supplementary data file 2 (8b elemental maps) Supplementary data file 3 (12a elemental maps)

Introduction

Supplementary data files include an extended method, a series of Tera-Wasserburg Concordia plots showing normalized standards (supplementary figure 1), a table detailing the instrument parameters used during LAICPMS analysis (supplementary table 1). Additional files include an excel spreadsheet with all normalized U-Pb data used in this paper and corresponding trace element concentrations for elementally mapped samples (8b and 12a)

Note: analyses have been culled from U-Pb data based on the following: association with cracks/contaminated material, low Pb counts and inconsistent time resolved Pb/Pb or U/Pb signals

Delete all unused file types below. Copy/paste for multiples of each file type as needed.

Extended Method

Laboratory Processing

Calcite samples were selected and cut (in ~1cm^3 blocks) to reveal internal sections that cross-cut the veins. Subsequently, the calcite pieces were mounted in 1-inch (2.5cm) round epoxy mounts using epoxy cure resin (5g epoxy resin and 1.15g epoxy hardener) and ground (using 800 and 2000 grit sandpaper) and polished (using a 3µm polishing cloth with diamond suspension fluid) to reveal a smooth surface.

Sample imaging was conducted at the British Geological Survey, Nottingham, UK. Cathodoluminescence imaging was conducted with a Technosyn 8200 MKII cold-cathode luminoscope stage attached to a Nikon optical microscope with a Nikon long working distance lens, and equipped with a Zeiss AxioCam MRc5 digital camera; vacuum and electron beam voltage and current were adjusted as required to generate optimum luminescence. Back-scattered electron and charge-contrast imaging were conducted using a FEI QUANTA 600 environmental scanning electron microscope (ESEM) with a working distance of 10 mm. BSE images were recorded using a solid-state (dual-diode) electron detector, with a 20 kV electron beam accelerating voltage, and beam currents between 0.1 and 0.6 nA,. Charge Contrast Images were recorded using a FEI large-field gaseous secondary electron (electron cascade) detector, with 20 kV electron beam accelerating voltage, and beam currents of 1.2 to 4.5 nA.

LA-ICP-MS U-Pb spot-analysis

LA-ICP-MS analysis was conducted at the University of Adelaide using an ASI resolution LR Laser Ablation System coupled to an Agilent 7900 mass spectrometer in order to determine U and Pb concentrations. Large spot sizes (110 microns) were selected in order to maximise the signals from elements that were expected to have low concentrations. Only isotopes necessary for U-Pb dating (^{43}Ca,^{202}Hg ^{204}Pb,^{206}Pb, ^{207}Pb,^{208}Pb,

^{232}Th and^{238}U) were measured during spot analysis in order to maximise the dwell time on masses expected to have low abundance, such as the isotopes of Pb. Standard-sample bracketing was used, with the NIST614 glass reference material used for fractionation correction of the Pb-Pb ratios, and the WC-1 calcite reference material (Age: 254.4 ± 6.4) for correction of the U-Pb ratios [*Li et al.* , 2014;*Roberts and Walker* , 2016; *Roberts et al.* , 2017]. An in house calcite sample labelled 'Prague' of known stratigraphic age (~424 Ma) was used as an accuracy check [*Farkaš et al.* , 2016]. In more detail, a correction factor was calculated based on the offset between the measured age and the known age of WC-1. This factor was then used to correct both the 'Prague' secondary standard and the unknowns.

LA-ICP-MS Elemental Mapping:

LAIPCMS elemental mapping was conducted to identify alteration and different growth zones. Before elemental mapping, the surface of samples was gently re-ground (using 2000 grit sandpaper) to just below the laser ablation pits. Following this the surface was re-polished (using a 3µm polishing cloth as before). Maps were created at the University of Adelaide using an ASI resolution LR Laser Ablation System coupled to an Agilent 7900 mass spectrometer (i.e. the same as U-Pb analysis). A square laser beam of 91x91µm was used to create line rasters on selected areas of calcite samples. Data reduction was conducted using Iolite software [*Paton et al.* , 2011]. Elemental map data was produced using the Monocle plugin for Iolite [*Petrus et al.* , 2017]. In more detail, polygons, termed regions of interest (ROI) [*Petrus et al.* , 2017] surrounding to ablation spots were used to query elemental concentrations. Some spot analyses were removed based on anomalous chemistry, particularly high Al and U.

Repeat for any additional Supporting Text

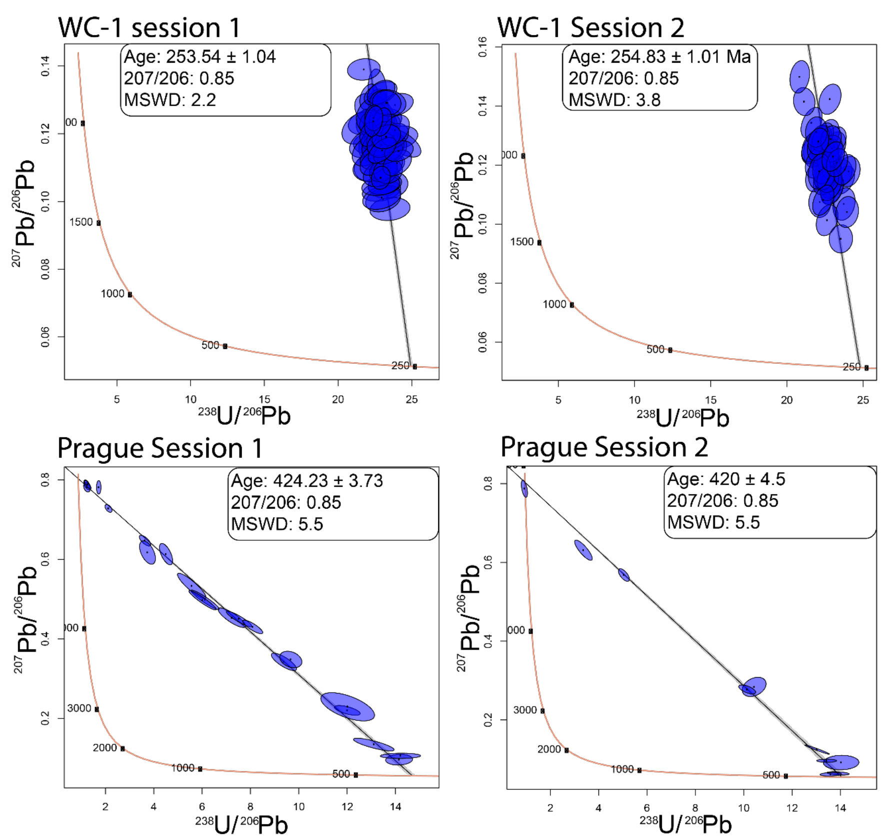

Figure S1. T-W Concordia plots showing secondary standards WC-1 and 'Prague' normalised to WC-1's correct age. Both WC-1 and 'Prague' regressions are anchored to the approximate Stacey and Kramers two stage Pb evolution model initial Pb composition (for Phanerozoic samples). Note 'Prague' secondary standard has a high failure rate due to significant zonation in U-Pb and Pb-Pb ratios in certain calcite chips.

Brand and Model	RESOlution-LR 193nm Excimer Laser System
Wavelength	193nm
Pulse Duration	20ns
Spot Size (U-Pb analysis)	110µm, (75µm - NIST614)
Spot Size (Elemental mapping)	91x91 (75µm NIST612)
Repetition Rate	10Hz
Energy Attenuation	100%T (50% NIST612)
Laser Fluency	8 j/cm^2
ICPMS	
Brand and Model	Agilent 7900x
Forward Power	1350W
Torch Depth	4.5mm
Gas Flows	
Plasma (Ar) Auxiliary (Ar)	15L/min 1L/min
Carrier (He)	07L/min
Sample (Ar)	0.88L/min
Data Acquisition Parameters	
Data Acquisition Protocol	Time resolved analysis
Scanned Isotopes (U-Pb analysis)	43Ca, 202Hg 204Pb, 206Pb, 207Pb, 208Pb, 232Th 238U
Scanned Isotopes (elemental mapping)	23Na, 25Mg, 27Al, 29Si, 43Ca, 55Mn, 56Fe, 88Sr, 130Ba, 139La, 140Ce, 141Pr, 1
Detector Mode	Peak Hopping, Pulse & Analog counting
Background Collection	30 (NIST612) 10 (mapping)
Ablation for Age Calculation	30 (ablation time for mapping varied by line length)
Washout	20
Standards	
Primary Standards (U-Pb analysis)	NIST614
Secondary Standards (U-Pb analysis)	WC-1, 'Prague'
Primary Standards (elemental mapping)	NIST612

Table S1. LA ICP MS parameters for U-Pb analyses and elemental mapping

Journal Pre-proofs

In-situ calcite U-Pb geochronology of hydrothermal veins in Thailand: new constraints on Indosinian and Cenozoic deformation

Alexander Simpson, Stijn Glorie, Chris K Morley, Nick M.W Roberts, Jack Gillespie, Jack K Lee

PII:	S1367-9120(20)30442-9
DOI:	https://doi.org/10.1016/j.jseaes.2020.104649
Reference:	JAES 104649

To appear in: *Journal of Asian Earth Sciences*

Received Date:	23 September 2020
Revised Date:	27 November 2020
Accepted Date:	29 November 2020

Please cite this article as: Simpson, A., Glorie, S., Morley, C.K., Roberts, N.M., Gillespie, J., Lee, J.K., *In-situ* calcite U-Pb geochronology of hydrothermal veins in Thailand: new constraints on Indosinian and Cenozoic deformation, *Journal of Asian Earth Sciences* (2020), doi: https://doi.org/10.1016/j.jseaes.2020.104649

In-situ calcite U-Pb geochronology of hydrothermal veins in Thailand: new constraints on Indosinian and Cenozoic deformation

Alexander Simpson[1], Stijn Glorie[1], Chris K Morley[2], Nick M W Roberts[3], Jack Gillespie[1,4], Jack K Lee[3,5]

[1]Department of Earth Sciences, The University of Adelaide, SA 5005, Australia

[2]Chiang Mai University, 239 Huaykaew Road, Tumbol Suthep Amphur Muang, Chiang Mai, Thailand

[3]Geochronology and Tracers Facility, British Geological Survey, Keyworth NG12 5GG, UK

[4]School of Earth and Planetary Sciences, Curtin University, WA 6845, Australia

[5]Department of Earth Sciences, University of Durham, Science Labs, Durham

Corresponding author: Stijn Glorie (stijn.glorie@adelaide.edu.au)

Abstract

U-Pb dating of calcite veins allows direct dating of brittle deformation events. Here, we apply this method to hydrothermal calcite veins in a fold-and-thrust belt and a large scale strike-slip fault zone in central and western Thailand, in an attempt to shed new light on the regional upper crustal deformation history. Calcite U-Pb dates for the Khao Khwang Fold and Thrust Belt (KKFTB) of 221 ± 7 Ma and 216 ± 3 Ma demonstrate that calcite precipitated during tectonic activity associated with stage II of the Indosinian Orogeny (Late Triassic – Early Jurassic). One additional sample from the KKFTB suggests that the Indosinian calcite has locally been overprinted by a Cenozoic fluid event with a different chemistry. For the Three Pagodas Fault Zone (TPFZ), our calcite U-Pb results suggest a complex, protracted history of Cenozoic brittle deformation. Petrographic information combined with contrasting redox-sensitive trace elemental signatures suggest that the vein arrays in the TPFZ precipitated during two distinct events of brittle deformation at ~48 and ~23 Ma. These dates are interpreted in the context of far-field brittle deformation related to the India-Eurasia collision. The presented calcite U-Pb dates are in excellent agreement with published age constraints on the deformation history of Thailand, demonstrating the utility of the method to decipher complex brittle deformation histories. The paper further illustrates some of the complexities in relation to calcite U-Pb dating and provides suggestions for untangling complex datasets that could be applied to future studies on the deformation history of Thailand and other regions.

Key Words:

Calcite U-Pb dating, LA-ICP-MS element maps, Indosinian Orogeny, India-Eurasia collision, Khao Khwang Fold and Thrust Belt, Three Pagodas Fault Zone

1 Introduction

A variety of techniques have been used to constrain the geological history of Thailand, from U-Pb and Ar-Ar dating of igneous and metamorphic minerals to biostratigraphy of syn-kinematic sequences and unconformable relationships (Hansen and Wemmer, 2011; Lacassin et al., 1997; Morley et al., 2011; Morley and Racey, 2011; Ridd et al., 2011; Ueno and Charoentitirat, 2011; Ueno et al., 2010). However, the exact timing of major tectonic events that affected Thailand, such as the onset and extent of the Indosinian Orogeny, remain controversial (e.g. Morley et al., 2013). Similarly, the timing of Cenozoic deformation, in relation lateral extrusion in response to the India-Eurasia collision (Rhodes et al., 2005) is established from biostratigraphic dating of sedimentary basins (as reviewed by Morley and Racey, 2011), from radiometric dating of ductile deformation in a limited number of localities (e.g. Gardiner et al., 2016; Lacassin et al., 1997; Watkinson et al., 2011), and from radiometric cooling ages inferred to be related to exhumation and erosion in response to fault motion (Morley, 2009; Nachtergaele et al., 2019; Upton, 1999). However, dating of individual structures in sedimentary sequences is typically rather imprecise and often it is difficult to justify whether a particular fault or fold in a Palaeozoic unit is related to Triassic or Cenozoic deformation. Inferences made in previous studies (e.g. Arboit et al., 2015; Morley, 2002; Morley et al., 2013; Rhodes et al., 2005) about the timing of such structures in Palaeozoic carbonates provide an excellent framework to both explore U-Pb dating of hydrothermal calcite veins and to enhance our understanding of the brittle deformation history of Thailand.

In this study, hydrothermal veins were targeted form two locations, the Khao Khwang Fold and Thrust Belt (KKFTB) and the Three Pagodas Fault Zone (TPFZ) (Fig. 1), which both record complex tectonic histories. The high-temperature tectonic history of both regions is relatively well studied. For the KKFTB, zircon U-Pb dates for granitoid intrusions (Dew et al., 2018a; Morley et al., 2013) and syn-tectonic Triassic sediments (Arboit et al., 2016b) as well as few K-Ar dates (~262-208 Ma) on authigenic illites within thrust fault zones (Hansberry et al., 2017), have provided age constrains on deformation attributed to the Indosinian Orogeny (Morley et al., 2013). Deformation along the TPFZ is constrained by mica Rb-Sr and Ar-Ar dates (~36 - 33 Ma) (Lacassin et al., 1997; Nantasin et al., 2012), while regional metamorphism and ductile deformation was dated by zircon and monazite U-Pb and mica Ar-Ar dates at ~48 – 40 Ma (Österle et al., 2019; Watkinson et al., 2011). Latter deformation event is attributed to extrusion tectonics, related to the India-Eurasia collision (Morley et al., 2011; Watkinson et al., 2011). In contrast, published age constraints on the low-temperature tectonic history of both the KKFTB and the TPFZ are rather scant and limited to apatite fission track dates, ranging between ~39 – 19 Ma, which suggest that low-temperature exhumation is Cenozoic in age, possibly related in part to strike-slip fault activity (Nachtergaele et al., 2019; Upton, 1999).

Both of the selected study areas contain extensive calcite veining, hosted within the Permian Saraburi group carbonate sequences and mixed siliclastic/carbonate formations (Dew et al., 2018b; Warren et al., 2014), that can be linked to major structures (e.g. Hansberry et al., 2015; Hansberry et al., 2014; Nazrul, 2015), which largely lack absolute (low temperature) time constraints on brittle faulting. Previous studies have demonstrated that *in-situ* laser ablation inductively coupled mass spectrometry (LA-ICP-MS) U-Pb dating of syn-tectonic calcite can produce direct constraints on the timing of calcite growth during brittle deformation (Hansman et al., 2018; Nuriel et al., 2017; Parrish et al., 2018; Roberts, 2018; Roberts and Walker, 2016).

While crack-seal calcite veins are preferable for dating due to their textural link to fault movement (Bons et al., 2012; Roberts and Walker, 2016), there are a range of possibly syn-tectonic calcite textures that are worth exploring with this technique. In areas with complex tectonic histories and multiple generations of calcite growth during deformation, previous studies (e.g. Beaudoin et al., 2018; Hansman et al., 2018; Parrish et al., 2018) have applied calcite U-Pb dating to unravel multiple deformation events in the same outcrop, even at the microscale (Goodfellow et al., 2017). Hence, the complex structural architecture of the KKFTB and TPFZ, where multiple deformation events might have caused fluid flow and associated calcite precipitation with distinct chemical compositions, forms an excellent natural laboratory to explore calcite U-Pb geochronology in relation to directly date brittle deformation. Here we present *in-situ* calcite U-Pb results for hydrothermal veins in both the KKFTB and TPFZ in Thailand, and we discuss how coupled calcite U-Pb dating with trace element mapping and detailed petrography can be used to differentiate different fluid generations associated with distinct deformation events in the study areas.

2 Geological setting and field site descriptions

2.1 Khao Khwang Fold and thrust Belt

2.1.1. Regional Tectonic setting

Thailand can be geologically subdivided into the Sibumasu Block (in the west) and the Indochina Block (in the east) (see Morley, 2018; Ridd et al., 2011; Sone and Metcalfe, 2008) (Fig. 1). These Blocks are separated by the remnants of an overthrust accretionary complex (The Inthanon Zone) and a Palaeozoic island arc (Sukhothai Arc) (Ridd et al., 2011) (Fig. 1). Given the similarity of its upper Palaeozoic stratigraphy with other Gondwana-derived terranes, the

Sibumasu Block likely represents a fragment of the northern margin of Gondwana, (Ueno et al., 2010). The Sibumasu Block likely rifted off Gondwana during the early Permian, before colliding with Indochina (as part of Eurasia) during the Paleo-Tethys closure (Barber et al., 2011; Dew et al., 2018a).

The Khao Khwang Fold and Thrust Belt (KKFTB) is situated on the western edge of the Indochina Block in the Saraburi Province (Fig. 2). The KKFTB is composed of deformed mixed siliclastic-carbonate sediments that were deposited during the Permian to early Triassic (Dew et al., 2018b) and is structurally characterised by WNW-ESE to NE-SW oriented thrusts and folds (Morley et al., 2013). Modern structural studies of the Khao Khwang Fold and Thrust belt were first summarized by Morley et al. (2013). At the time of this study it was thought that all the sedimentary units related to the Indosinian orogeny were of Permian age, while a belt of Permo-Triassic volcanics lay immediately to the south. Consequently, there appeared to be no syn-orogenic sedimentary units preserved to help date deformation. The age of deformation was estimated from regional considerations based on three main criteria (as reviewed in Morley et al. (2013)): 1) the timing and nature of granitic intrusions (i.e. Andean margin-related I-type, post-collisional S-type), 2) the timing of metamorphism in amphibolite to granulite grade rocks, and 3) the timing of Triassic unconformities identified from outcrop and seismic data in the Khorat Plateau area. The Triassic unconformities were the most important control because they were translated from a part of the Indochina block that was located only about 150 km NNE of the KKFTB. Outcrop and seismic reflection data demonstrated that in the Khorat Plateau area all the major Indosinian contractional deformation had finished prior to deposition of Norian-age continental sedimentary rocks of the Kuchinarai Group (Booth and Sattayarak, 2011). The unconformity between the deformed Permian section and the Kuchinarai Group is marked by a widespread basal limestone conglomerate, and is known as the Indosinian I unconformity (Booth and Sattayarak, 2011). However, this evidence just limited the timing of deformation to sometime between the end of deposition in the Late Permian, and the Norian (i.e. between about 260 Ma and 210 Ma).

Dating of detrital zircons from the Saraburi Group resulted in re-assignment of the upper boundary from the Permian to the Triassic, with a maximum depositional age of 251±3 Ma (Arboit et al., 2016b). This unit is strongly folded and exhibits axial planar, slaty cleavage, indicating a younger deformation event than ~251 Ma. A younger Triassic unit was also identified, with a maximum depositional age of 205±3 Ma, which is folded and contains pencil cleavage, indicating that some deformation in the KKFTB post-dates that in the Khorat Plateau (Arboit et al., 2016b). In addition, andesitic dikes and sills frequently cross-cut the Saraburi Group and some of these intrusions are deformed by thrusts and folds, while others cross-cut structures (Arboit et al., 2016a). Unfortunately, most of these intrusions lack zircons, and are too altered to be radiometrically dated (Arboit et al., 2016a), and, therefore, have proven not particularly useful to constrain deformation. However, K-Ar dating of authigenic illite from fault zones was attempted in one quarry (Siam Cement Quarry), where major faults in shale-prone section are well-exposed (Hansberry et al., 2017). Three K-Ar dates (230±5 Ma, 225±5 Ma, 209±4 Ma) interpreted to be related to fault activity, were obtained, indicating that structural activity in the Sarabui Group lasted at least between ~230 Ma and ~205 Ma. There are also later, cross-cutting strike-slip faults, which are probably of Cenozoic age, but their timing is largely unconstrained.

Calcite veins have formed in a variety of structural and sedimentary stages during development of the Saraburi Group including: 1) early diagenesis and burial during Permian deposition (marine cements), 2) during different stages of folding and thrusting of the Indosinian orogeny, 3) along the margins of igneous intrusions, 4) within strike-slip fault zones, and 5) during late Neogene karstification. Stable ^{18}O and ^{13}C isotope values measured from over 1000 veins in the Saraburi Group have established the different categories of veins form distinct trends on the stable isotope cross plots (Warren et al., 2014). These categories include (Warren et al., 2014): pre-deformation burial (eogenesis and early mesogenesis); early stage Indosinian deformation/deformation away from high strain zones (mesogenesis); later stage Indosinian deformation where the rock matrix became impermeable and fluid flow along large thrusts tapped deeper, hotter fluids; and late stage (Neogene) meteoric mixing – uplift and telogenesis (Fig. 2).

The temperature of deformation affecting the Saraburi Group has been estimated in a number of ways (cleavage type, calcite twin morphology, vitrinite reflectance, illite crystallinity), and the approximate estimates based on the latter two techniques range between 160-220° C ± 20° C (Hansberry et al., 2015). Calcite twins range between Type I (thin twins), Type II (tabular thick twins), as well as Type III (bent twins) following the nomenclature of (Burkhard, 1993). This indicates lower anchizonal temperatures (<250°C; Burkhard, 1993; Ferrill et al., 2004).

2.1.2. Sample localities

Thirteen calcite samples were collected for U-Pb dating from a variety of geographic localities within the KKFTB. Unfortunately, the majority of these samples did not produce useful calcite U-Pb dates (large uncertainties) due to the low concentrations of uranium in the samples (success rate of 23%). The localities that yielded useful results (Table 1) are described below. Samples 7b and 8b were taken from quarries that are 7 km apart (Fig. 3) in the western part of KKFTB (Figs. 2 and 3), with a predominantly southerly vergence (Fig. 3D). Sample 10b was taken from the eastern part of the KKFTB (Fig. 2), where the vergence is predominantly to the north.

2.1.2.1. Samples 7b

Sample 7b is from a broad anticlinal area that lies in the footwall of a large fault propagation fold (Fig. 3). In this area most bedding surfaces are modified by pressure dissolution, and numerous calcite veins are exposed, both at high angles to bedding as well as parallel to bedding. Some low displacement (< 20 m throw) thrusts affect the section, with one thrust exhibiting a beheaded anticline (i.e. the thrust cuts through the backlimb and the forelimb) in its hanging wall (Fig. 4).

2.1.2.2. Sample 8b

The quarry where sample 8b was taken has two main areas (Fig. 3). The western area exhibits a low-angle, south-dipping thrust (T1, Fig. 4B), which is cut by a later steeply inclined (dip 65° ESE), oblique thrust (T2, Fig. 4B). A NW-SE striking, sub-vertical strike-slip fault is present in the eastern area. This fault exhibits sub-horizontal slickensides and is inferred to be either younger than the two thrusts, or possibly contemporaneous with T2 as part of a conjugate set of strike-slip faults. Sample 8b was taken from a heavily brecciated limestone, whose clasts float in a network of veined material (Fig. 4C).

2.1.2.3. Sample 10b

The quarry for sample 10b has two faces, the northerly face exhibits an exposed, steeply-dipping (70°SSW) bedding surface (Fig. 5B), while the western face is a dip-section (Fig. 5C). The bedding surface exposes bed-perpendicular veins that strike in a N-S direction (Fig. 5B). These are interpreted as early-formed veins that developed prior to the folding event that rotated bedding. Sample 10b was sourced from a bed-parallel, striated vein that is associated with bedding plane slip that produced a small duplex structure in the limestone beds (Fig. 5C). The early N-S striking bed-perpendicular veins are rotated by the later large-scale folding, and also locally within the duplex structure (Fig. 5C).

2.2 Three Pagodas Fault Zone

2.2.1. Regional setting

Situated within Kanchanaburi Province, the Three Pagodas Fault Zone (TPFZ) is characterised by a series of NW-SE trending strike-slip faults (Morley, 2002; Rhodes et al., 2005) (Fig. 1) and is estimated to be a ~30 km in width and more than 700 km in length (Searle and Morley, 2011). In more detail, the TPFZ comprises numerous brittle fault strands, that predominantly cut through Permian and Ordovician limestones, as well as other lithologies including Triassic and Cenozoic clastics, and a limited region of metamorphic rocks (gneisses, calc-silicates, schists) (Morley, 2002; Rhodes et al., 2005) (Fig. 1).

Two episodes of cooling, attributed to exhumation, are documented by regional apatite fission track (AFT) studies at ~39 – 32Ma and ~24 – 19Ma (Upton, 1999), and both are thought to be related regionally to deformation arising from the India-Eurasia collision and convergence (Rhodes et al., 2005). The first exhumation period coincides with mica Rb-Sr and Ar-Ar dates (~36 - 33 Ma) that are interpreted as being related to the late or final stages of Eocene – early Oligocene ductile left-lateral slip along the TPFZ (Lacassin et al., 1997; Nantasin et al., 2012). Furthermore, dating of syn-kinematic minerals in their structural context (restraining bends) (e.g. Lacassin et al., 1997; Palin et al., 2013) have been used to infer initial left-lateral transpressional activity (~39 – 32 Ma) along the TPFZ as well as the parallel Mae Ping Fault Zone (Fig. 1; Morley et al., 2007).

More regionally, U-Pb dating of zircon rims and monazites hosted in an augen gneiss exposed in the Mae Ping Fault zone suggest an earlier metamorphic event at ~45 Ma (Österle et al., 2019). Eocene tectonic activity (at ~48 Ma) has been identified on the nearby Ranong and Khlong Marui Faults (Fig. 2) as well (Watkinson et al., 2011), suggesting this was a regional deformation event. Sinistral movement along the TPFZ was followed by a change to dextral transtensional activity (~24 Ma to present), as indicated by the development of pull-apart basins at releasing bend configurations (Morley, 2002; Morley et al., 2011; Morley and Racey, 2011; Rhodes et al., 2005). The continued movement of India into Eurasia and resultant changes to the regional stress field have been posited as an explanation for the change from sinistral to dextral deformation (Huchon et al., 1994; Leloup et al., 2001; Rhodes et al., 2005).

Three calcite veins were sampled within the TPFZ, aiming to enhance our understanding of the role of strike-slip faulting during Cenozoic deformation, and how strike-slip fault patterns have evolved with time. Only one sample produced sufficiently high U concentrations to calculate a calcite U-Pb date.

2.2.2. Sample description: Sample 12a

Within the overall NE-SW trending TPFZ are two major strike-slip fault strands that have N-S trending segments that acted as releasing bends during dextral motion, and these have given rise to low-lying areas corresponding with Cenozoic pull-apart basins (Fig. 6; Morley and Racey, 2011). These areas have been dammed and are now water reservoirs. Samples were taken from an outcrop along Highway 3199 (Table 1), which runs along the TPFZ, near the Srinagarind Dam and reservoir (Fig. 6A). The outcrop section is composed of dark grey to medium grey, fine-grained bedded Ordovician limestone that is strongly boudinaged (Fig. 6). These 'boudins' are tens of meters in length and 30 – 40 cm wide and host numerous calcite veins, from which sample 12a was taken (Fig. 6C). Long, sub-horizontal striations mark bounding surfaces of the boudins (fig. 6B, C), which strongly suggest they are related to strike-slip motion. In addition, the boudinaged layers are folded (Fig. 6), indicating they developed prior to, or accompanied folding. Hence, calcite dating will allow to constrain the timing of regional deformation, associated with fault activity in the TPFZ.

3 Materials and Methods

Of the sixteen samples that were screened for this work, only four samples provided useful U-Pb dates (Table 1); these are the only samples considered further. Unsuccessful samples fall into the following two categories: (1) samples dominated by high common Pb; and (2) samples containing very low uranium concentrations, producing too high analytical uncertainties that render an accurate regression impossible (samples with average U concentrations below 0.1 ppm were discarded for this study).

Selected calcite fragments from each sample were mounted in 1 inch epoxy mounts (for some samples multiple fragments were analysed). Sample imaging was conducted at the British Geological Survey, Nottingham, UK. Cathodoluminescence (CL) imaging was conducted with a Technosyn 8200 MKII cold-cathode luminoscope stage attached to a Nikon optical microscope with a long working distance lens, and equipped with a Zeiss AxioCam MRc5 digital camera. Vacuum and electron beam voltage and current were adjusted as required to generate optimum luminescence. Back-scattered electron and charge-contrast imaging were conducted using a FEI QUANTA 600 environmental scanning electron microscope (ESEM) with a working distance of 10 mm. BSE images were recorded using a solid-state (dual-diode) electron detector, with a 20 kV electron beam accelerating voltage, and beam currents between 0.1 and 0.6 nA. Charge Contrast Images (CCI) were recorded using a FEI large-field gaseous secondary electron (electron cascade) detector, with 20 kV electron beam accelerating voltage, and beam currents of 1.2 to 4.5 nA.

LA-ICP-MS element mapping and U-Pb dating was conducted at The University of Adelaide using an ASI resolution LR Laser Ablation System coupled to an Agilent 7900 mass spectrometer. First the samples were mapped for a suite of trace elements (details in Table 2) in order to identify zones with suitable U and Pb concentrations for dating purposes, as well as to identify growth zoning or alteration. Subsequently, spot analysis was conducted for U-Pb dating (in two analytical sessions) using large spot sizes (110 µm diameter, ~45µm depth) in order to maximise the signals from elements that were expected to have low concentrations. Instrumental settings for all runs are included in Table 2. Only isotopes necessary for U-Pb dating (^{43}Ca, ^{202}Hg

^{204}Pb, ^{206}Pb, ^{207}Pb, ^{208}Pb, ^{232}Th and ^{238}U) were measured during spot analysis in order to maximise the dwell time on masses expected to have low abundance, such as the isotopes of Pb. The concentrations of other trace elements (such as Al, Si, Mn, Ce) associated with each spot analysis were calculated from the element maps (explained further below). Standard-sample bracketing was used, with the NIST614 glass reference material used for fractionation correction of the Pb-Pb ratios, and the WC-1 calcite reference material (for correction of the U-Pb ratios (Li et al., 2014; Roberts et al., 2017; Roberts and Walker, 2016). The resulting correction factors for the U/Pb ratios were calculated at 0.95 for session 1 and 0.91 for session 2 and are in good agreement with typical values obtained in Roberts et al. (2017). An in house calcite sample from a limestone unit in the Prague basin of known stratigraphic age (~424 Ma), labelled 'Prague' was used as a secondary material to check accuracy (Farkaš et al., 2016) (see Supplementary File 1). After the normalisation procedures, the calcite U-Pb ages for the 'Prague' secondary standard were calculated at 424.2 ± 3.7 Ma and 423.9 ± 4.4 Ma, which are in excellent agreement with the published age, cited above.

Data reduction was conducted using Iolite software (Paton et al., 2011). The trace element maps were produced using the Monocle plugin for Iolite (Petrus et al., 2017). From these maps, polygons, (termed regions of interest; Petrus et al., 2017) surrounding the ablation spots were used to query elemental concentrations. Some spot analyses were removed based on anomalous chemistry related to alteration or different mineral phases (e.g. clays), particularly high Al and U. Resulting calcite U-Pb dates were calculated using isochron regressions in IsoplotR (Vermeesch,

2018) and are presented in Tera-Wasserburg plots (the relevant isotope ratios can be found in Supplementary File 2).

4 Results

4.1 Sample characterization

4.1.1 KKFTB samples

Samples 7b and 10b exhibit simple euhedral calcite growth that is commonly found in primary fracture-filling calcite (Bons et al., 2012).

Sample 8b reveals a clear primary cleavage that appears to be cross-cut by later veinlets. These later veinlets are enriched in many trace elements such as Al and Mn (Fig. 7). The CL texture of the vein is fairly weak and homogeneous, except for the younger veinlets which are darker. CCI shows a planar fabric that is pervasive throughout the primary calcite at a shallow angle to the cleavage (Fig. 7). This fabric is interpreted as low-temperature deformation twinning of Type 1 or 2 due to the apparent narrow width of the twins and lack of recrystallization (Ferrill et al., 2004).

4.1.2 TPFZ sample

Sample 12a is a veinlet hosted within a limestone matrix. The crystal/grain boundaries are ragged, and may reflect overprinting during successive fluid-flow and/or a deformation events. The calcite has a very low CL response, and therefore, calcite crystal outlines and primary growth zoning cannot be ascertained (Fig. 8). In CCI, the calcite exhibits a planar fabric that is patchy in nature (Fig. 8). We interpret this to reflect high-temperature twinning (Type IV; Ferrill et al., 2004), and dynamic recrystallization. Zonation patterns in Ce and Mg appear to correlate with the crystal boundaries that are visible in reflected light (Fig 8).

4.2 U-Pb dating and trace element geochemistry

Average trace element concentrations are presented in Table 3. The U and Pb concentrations for the spot analyses across the four successful samples range from 272 to 753 ppb and 34 to 131 ppb, respectively. Individual trace element data can be found in Supplementary File 2.

4.2.1 KKFTB samples

Sample 7b yields a lower intercept age of 221 ± 7 Ma with an MSWD of 2.1, based on 54 spot analyses (Fig. 9). The upper intercept $^{207}Pb/^{206}Pb$ composition determined from the unconstrained regression in Tera-Wasserburg plot is 0.6225 ± 0.0183. Sample 10b yields a lower intercept age of 217 ± 2 Ma, with an MSWD of 1.7, based on 84 spot analyses. The upper intercept $^{207}Pb/^{206}Pb$ ratio for this sample is 0.7092 ± 0.0099. Sample 8b yields a scattered array of data in Tera-Wasserburg space. The Mn concentration map for the sample reveals distinct zonations (Fig. 7), which were used to group the U-Pb data into separate populations. The U-Pb data obtained from Mn-rich zones in the calcite sample (population A) define a regression line with a lower intercept U-Pb age of 31 ± 6 Ma (MSWD = 3.7, 14 analyses, 115-155 ppm Mn). In contrast, the U-Pb data for ablation targets in Mn-poor zones (population B) define a regression line with a lower intercept age of 197 ± 9 Ma (MSWD = 4.4, 10 analyses, 72-112 ppm Mn). The few open ellipses between those two populations are associated with boundaries between high and low Mn zones (Figs. 7, 9). The upper intercept $^{207}Pb/^{206}Pb$ compositions for populations A and B are 0.765 ± 0.059 and 0.769 ± 0.097, respectively (Fig. 9). Few additional data points were discarded based on significantly elevated Al and/or U concentrations (proxy for detrital input) associated with cracks through the calcite crystals (Fig. 7).

4.2.2 TPFZ sample

Sample 12a yields a scattered array in Terra-Wasserburg space. The Ce concentration map for the sample reveals distinct zonations (Fig. 8), which were used to group the U-Pb data into two populations. The U-Pb data obtained from Ce-poor zones in the calcite sample (population A) define a regression line with a lower intercept U-Pb age of 23 ± 1 Ma (MSWD = 2.4, 22 analyses, 0.9-2.2 ppm Ce). The U-Pb data for ablation targets in Ce-rich zones (population B) define a regression line with a lower intercept age of 48 ± 4 Ma (MSWD = 3.6, 18 analyses, 2.2-9.2 ppm Ce). (Figs. 8, 9). The upper intercept compositions for populations A and B are 0.665 ± 0.0157 and 0.691 ± 0.029, respectively (Fig. 9). Few additional data points were discarded based on significantly elevated Al and/or U concentrations (proxy for detrital input) associated with cracks through the calcite crystals (Fig. 8).

5 Discussion

5.1 Initial lead compositions and fluid sources

All of the samples dated show significantly lower initial (i.e. common) Pb ratios ($^{207}Pb/^{206}Pb$) than would be expected based on the traditional two part terrestrial evolution model of the earth (~0.83-0.86 for Meso-Cenozoic samples; Stacey and Kramers, 1975). This indicates that the fluids from which the calcite precipitated contained abundant radiogenic lead. The Ordovician host limestones have very low U concentrations and an initial $^{207}Pb/^{206}Pb$ ratio of 0.839 ± 0.02

(Supplementary File 2), which is conform with the Earth reservoir at that time (Stacey and Kramers, 1975). Hence, it is unlikely that the fluids were sourced from the Ordovician host rocks as the low U concentrations in the limestones cannot have generated particularly radiogenic values in the required timeframe between Ordovician deposition and Meso-Cenozoic fluid precipitation. Warren et al. (2014) suggested that both Indosinian and Cenozoic carbonate veins were associated with deep and relatively hot fluids (strongly negative $\delta^{18}O$ and $\delta^{13}C$ values) (Fig. 10). Hence, it is more likely that a significant amount of deep-seated fluid-rock interaction occurred prior to vein precipitation. Thermally activated Pb loss after calcite precipitation is considered unlikely as an explanation for the low initial Pb ratios, because diffusive mobility of Pb is very slow at brittle conditions at temperatures below ~400°C (Cherniak, 1997).

5.2 Timing of the Khao Khwang Fold and Thrust Belt

Sample 7b was taken from a minor thrust fault in the footwall of a fault propagation fold in the KKFTB (Figs. 2, 3), which was hypothesised to have been active during the late Indosinian Orogeny. The obtained calcite U-Pb date of 221 ± 7 Ma (Fig. 9) confirms this hypothesis. Structural observations suggest that sample 10b was sourced from a bedding-parallel vein that formed in relation to flexural slip and folding. This sample (10b) gave the most precise age of the successfully analysed samples (216 ± 2 Ma), confirming that flexural slip and folding occurred during the Indosinian Orogeny. In more detail, the calcite dates for both locations have overlapping analytical uncertainties and constrain the timing of calcite growth in both locations to the Indosinian II deformation phase (~220 – 190Ma; Morley et al., 2013).

Sample 8b was taken from a heavily brecciated vein in close proximity to a strike-slip fault, where field observations indicate that this fault was most likely active during the Cenozoic.

Element mapping of sample 8b revealed the presence of high Al and elevated U (up to 1500% increase) along cracks (Fig. 7). We interpret this as due to the presence of an Al-rich mineral phase (such as a clay mineral) or alteration due to fluid flow along the cracks, and thus such data were discarded. The sample is of particular interest due to the presence of multiple U-Pb data populations (Fig. 9), that are associated with differences in Mn concentrations (Fig. 7). In more detail, a U-Pb age of 197 ± 9 Ma was obtained for analyses in Mn-poor zones of the calcite sample, while the U-Pb analyses in Mn-rich zones produced a much younger U-Pb age of 31 ± 6 Ma (Fig. 9). Ablation targets that were set close to boundaries between high and low Mn zones produced mixing ages between both populations (Fig. 7, 9).

Chemical zonation within calcite may represent changes in fluid chemistry (and thus potentially different fluid-flow events), or changes in uptake of metals (e.g. Barker and Cox, 2011; Paquette and Reeder, 1995; Reeder et al., 1990). Experimental evidence (Frank et al., 1982) demonstrates that Mn can show oscillatory zoning during calcite growth, related to uptake of Mn^{2+} along the calcite crystal surface that inhibits crystal growth. In fact, Mn zonation is the main source of luminescence for calcite in CL imaging (Frank et al., 1982). Mn zonation in sample 8b, however, does not correspond to oscillatory growth patterns (Fig. 7). Given this absence of oscillatory growth patterns and the association between Mn zonation and age populations, we consider it more likely that this zonation reflects changes in fluid chemistry between different precipitation/alteration events. It is, therefore, interpreted that the calcite initially grew during the Indosinian Orogeny (older age population with a poorly defined age of ~197 Ma), and that parts were subsequently recrystallised or altered in a fluid with a higher Mn concentration, associated with a Cenozoic deformation phase (poorly defined ~31 Ma age population). The mixing ages (open ellipses in Figure 9) can then be interpreted as being partially reset Indosinian ages in response to Pb mobility associated with the younger, Cenozoic, Mn-rich fluid infiltration.

The ~197 Ma age population (B) in sample 8b corresponds to calcite growth during Indosinian Orogeny stage II (Morley et al., 2013), similar as found for other locations in the KKFTB (samples 7b and 10b). The younger ~31 Ma age population of Sample 8b corresponds with apatite fission track ages (~39-19 Ma) in the vicinity (Upton, 1999), as well as with Ar-Ar and U-Pb dates on Cenozoic structures such as the MPFZ (Lacassin et al., 1997; Fig. 10). Therefore, following the interpretation given for the AFT and Ar-Ar dates, sample 8b may record evidence for calcite (re-)growth during Cenozoic reactivation that can be linked to the far-field effects of the India-Eurasia collision (Rhodes et al., 2005).

Prior to direct dating of structures using K-Ar dating of authigenic illite (Hansberry et al., 2017; Fig. 10), and now U-Pb dating of calcite, it was thought that the timing of major contractional deformation in the KKFTB was similar to the Khorat Plateau, i.e. of Indosinian I age, with little deformation occurring during Indosinian II (e.g. Morley et al., 2013). However, the initial results, of this study, and Hansberry et al. (2017), combined with identification of Triassic syn-kinematic sediments (Arboit et al., 2016a, Fig. 10), now point to significant deformation during Indosinian II.

5.3 Timing of the Three Pagodas Fault Zone

The timing of the boudin structures in the outcrop along the Three Pagodas Fault Zone was ambiguous from outcrop relationships alone because they, along with bedding, are rotated by short wavelength (10’s m) folds that could either be Cenozoic or Triassic in age. U-Pb dating of calcite is likely to be the only direct method available to resolve this issue with absolute constraints. Successful age determinations were obtained from one of the 'boudin' like zones from sample 12a, which can be described as a 'floating clast breccia zone', bounded by pressure solution seams. This sample likely formed from repeated fracturing related to activity along the fault zone. The analysed section of the sample is an area where multiple veins intersect with distinctive different trace element compositions (Fig. 8). Particularly, the Ce concentration map reveals distinct zonations in the sample (Fig. 8). Therefore, the resulting U-Pb dates for this sample were grouped into two populations associated with Ce-poor (population A) and Ce-rich (population B) zones (Figs. 8, 9). Population A was dated at 23 ± 1 Ma, which correlates with the beginning of a proposed period of dextral motion along the TPFZ at ~23.5 Ma (Lacassin et al., 1997). Population B was dated at ~48 Ma, which correlates with a major period of ductile shear along the nearby Ranong and Khlong Marui faults (~48-40 Ma; Fig. 10) (Watkinson et al., 2011). Similar U-Pb ages from zircon rims, of ~57 – 51 Ma (Nantasin et al., 2012) and ~45 Ma (Österle et al., 2019) have been obtained regionally within metamorphic complexes exhumed along strike-slip faults (Fig. 10). Morley (2012) proposed that an early (i.e. >40 Ma) phase of transpressional deformation affected a large region of central Thailand and adjacent countries, and this deformation may not be as strongly linked with escape tectonics as the later deformation. The ~48 Ma calcite U-Pb age for sample 12a, provides encouragement that U-Pb dating of calcite veins can help better define deformation patterns associated with brittle faults during this early stage of deformation.

Zonations in REE patterns (e.g. Ce/Yb ratios) have been used previously to distinguish between different calcite generations (Maskenskaya et al., 2013). Furthermore, REE distributions have been proposed as a proxy for diagenetic fluid properties, similar to $\delta^{18}O$ (Bons et al., 2012). Experimental studies suggest that the LREEs, especially Ce (and Eu), are highly mobile in fluids and are commonly used to track fluid sources (Migdisov et al., 2016; Brugger et al., 2016), thus it is inferred that the changes in LREE concentration for this study represent the variable chemistry of different episodes of calcite precipitation. While Ce was identified as a possibly indicator of extrinsic fluid properties (fluid-fluid/rock mixing or different fluid episodes) by Barker and Cox (2011), it was also noted that sector zoning in REEs may occur during precipitation. Thus REE zonation on its own may not be enough to conclusively distinguish between different hydrofracturing events.

Sample 12a shows extensive twinning, which is patchy along its length, reminiscent of high temperature dynamic recrystallization textures. The apparent thickness (based on polished chips), has a width > 5 µm, suggesting Type IV high temperature twins (Fig. 8). These twins would most likely have formed with temperatures exceeding 250˚C (Ferrill et al., 2004). Twinning overprints some of the elemental zonation and grain boundaries, and is thus considered to have occurred at the same time or after the latest (population A) generation of calcite growth/alteration. Thus, the twinning implies that the Cenozoic deformation, as young as ~23 Ma, occurred at maximum temperatures in excess of 250˚C. This is consistent with regional Ar-Ar biotite geochronology (~24 Ma) in the vicinity of the sample location, which implies cooling below ~300^{o}C (Lacassin et al., 1997). The similarities between dates and temperatures for calcite and biotite growth, implies twin formation occurred during or soon after the ~23 Ma episode of calcite precipitation.

Overall, our data suggest a protracted crystallisation or fluid-based resetting of calcite from at least ~48 to ~23 Ma. A key tenet of this dating method is to determine whether fluid-flow can outlast brittle deformation, which would limit the utility of the method for dating the latter. It is always difficult to rule this out, but in this study the correlation between age and chemistry, and the existence of the high temperature twins, suggests that the different ages do not simply represent U-mobility due to fluid-based alteration. Instead, the different calcite age populations reflect different fluid infiltration events with different fluid chemistries, during successive fracturing events, which occurred under high temperature conditions.

6 Conclusions

(1) Calcite U-Pb dates for the KKFTB have identified specific fracturing events occurring at ~221-217 Ma, associated with deformation during Stage II of the Indosinian Orogeny. This is in contrast with the predominantly Stage I deformation in the adjacent Khorat Plateau area. A larger data set is required to fully constrain the timing of deformation events in this area.

(2) Calcite U-Pb dates for the TPFZ reveal two generations of calcite growth at ~48 Ma and ~23 Ma, which are consistent with the timing of a ~52-45 Ma phase of sinistral displacement and an early stage of dextral motion at ~23-18 Ma. The ages are snapshots, of a more prolonged history of displacement on the fault zone, and are an encouraging indication that a more comprehensive calcite dating study would provide rewarding information about the history of the TPFZ.

(3) This study further highlights the use of reflective light microscopy and trace element mapping to unravel complex U-Pb calcite data, as discussed in Roberts et al. (2020). In particular, elemental mapping of redox-sensitive (and fluid mobile) elements such as Mn and REEs, have proven useful to detect distinct events of calcite growth that can be linked to different deformation events.

Acknowledgments

This study was supported by an Australian Research Council Discovery grant (DP150101730) and a University of Adelaide student support grant. Sarah Gilbert is thanked for assistance with the LA-ICP-MS facility. Two anonymous reviewers are thanked for their constructive feedback. Uwe Ring and a third anonymous reviewer are thanked for their constructive comments on an earlier draft of this manuscript.

Figure Captions

Figure 1. Simplified geological map of Thailand with indication of the Khao Khwang Fold and Thrust Belt (KKFTB) and Three Pagados Fault Zone (TPFZ) sampling areas (Based on Sone and Metcalfe, 2008; Warren et al., 2014).

Figure 2. Geological map of the Khao Khwang Fold and Thrust Belt (KKFTB) sampling area, showing the location of sample 10b, and the location map (Fig. 3) for samples 7b and 8b (modified from Morley et al., 2013 and Arboit et al., 2016a). Age data are zircon U-Pb ages from Morley et al. (2013).

Figure 3. A) Map of the Western part of the Khao Khwang Fold and Thrust belt around Na Phra Lan, showing the locations of samples 7b and 8b (modified from Warren et al., 2014). B = Satellite image of the quarry where sample 8b was taken (see A for location). C = Satellite image of Khao Yai, where sample 7B was taken (see A for location). D) Cross-section showing the structural context of the two sample areas, see A for location.

Figure 4. A) Interpreted photographs of the quarry where sample 7b was taken, showing relatively late north-vergent thrusts that truncate both limbs of secondary folds. Sample 7b was taken form folds associated with the beheaded anticline. **B**) West side of the quarry where sample 8b was taken showing an early low-angle thrust (T1), cut by a later high angled, oblique-

slip thrust (T2). **C**) 'Explosion' breccia from east side of quarry (sample 8b). See Fig. 2 for locations

Figure 5. Location details for sample 10b. A) Satellite image of the quarry where sample 10b was taken (see Fig. 2 for location). B) Photograph of north quarry face. C) Photograph of west quarry face where sample 10b was taken.

Figure 6. **A)** Topographic image showing the Three Pagodas Fault zone, and the locality of sample 12a. The numerous linear topographic features are typically indicative in this area of strike-slip faults. **B**) Overview photograph of the road outcrop of Ordovician limestone along Highway 3199 where sample 12a was taken. Beds a, b, c, d are boudinaged lighter grey beds. **C**) close-up image of bed b (located on part B): Veinlets within the central boundinaged area, from where sample 12a was taken, bounded by ~ 1 cm thick striated veins. Note the absence of veins in limestone above and below the boudinaged bed. **D**) Sketch of the key features of the boudin shown in C.

Figure 7. Images of KKFTB sample 8b. **a:** High resolution reflected light image with the green rectangle outline showing the area for the element maps. The white dashed outline refers to the area for image g. Spot ablation targets are indicated by circle symbols with a colour code that corresponds to different Mn concentrations (image c) and different age populations (see Figure 9). Blue targets are associated with elevated Mn concentrations (115-155 ppm) and younger calcite U-Pb ages. Yellow targets are associated with lower Mn concentrations (72-112 ppm) and older calcite U-Pb ages. White targets are located at the boundary between high and low Mn zones (image c) and return mixed ages (Fig. 9). **b:** Al element map. **c:** Mn element map. **d:** La element map. **e:** U element map. For all element maps warmer colours correspond to higher

concentrations and cooler colours correspond to lower concentrations. White circles show laser spot locations. **f:** Cathodoluminescence (CL) image, corresponding to a slightly larger area than that elemental mapped. Dark circles correspond to ablation spots. **g**: Charge Contrast Image (CCI) of sample 8b interpreted to show type I/II low temperature twins.

Figure 8: TPFZ sample 12a. **a:** Reflected light image with the green rectangle outline showing the elemental map area. Two different textures of calcite can be identified; 'twinned calcite' that has been successfully analyzed and fine grained, mottled calcite that returned common Pb dominated analyses. Spot ablation targets are indicated by circle symbols with a colour code that corresponds to different Ce concentrations (image d) and different age populations (see Figure 9). Yellow targets are associated with elevated Ce concentrations (2.2-9.2 ppm) and older calcite U-Pb ages. Blue targets are associated with lower Ce concentrations (0.9-2.2 ppm) and younger calcite U-Pb ages. The dashed outline shows the area for image b. **b:** Close up Charge Contrast Image (CCI) demonstrating type IV high temperature twins and dynamic recrystallization. **c:** U element map. **d:** Ce element map. **e:** Mg elemental map. **f:** Si elemental map. For all elemental maps warmer colours correspond to higher concentrations and cooler colours correspond to lower concentrations. Ablation targets are indicated on each element map by white symbols.

Figure 9. Tera-Wassurburg Concordia plots of samples 7b, 8b, and 10b from the KKFTB and sample 12a from the TPFZ. The concentration scale for sample 8b is expressed as log(Ce ppm), capped at 0.6 to remove outliers. The concentration scale for sample 12a is expressed as log(Mn ppm), capped at 2.15 to remove outliers. Each ellipse represents the 2σ uncertainty on the $^{207}Pb/^{206}Pb$ and $^{238}U/^{206}Pb$ ratios for individual laser spots. Uncertainties on the lower intercept ages are at 95% confidence level. Open ellipses show analyses removed due to probable contamination / mixing. All plots made using isoplotR (Vermeesch, 2018).

Figure 10. Summary of key evidence used to date tectonic events in the KKFTB and TPFZ. The calcite U-Pb dates from this study are indicated on the top row of the diagram. K-Ar illite dates are from samples in fault gouges (Hansberry et al., 2017). Stratigraphic ages are A = possible age range of the Indosinian I unconformity with I1 = oldest likely age and I2 = youngest age (late Norian) (Booth and Sattayarak, 2011). 1 = age of late syn-orogenic deposits (Hua Hin Late Formation equivalent), in Arboit et al. (2016b). For the TPFZ, the only stratigraphic inference available, is the similar timing to the Mae Ping Fault. There are two basins related to the releasing bend development of the TPFZ, but they are buried, and not well exposed. They are assumed to be of Late Oligocene-Miocene age (Morley and Racey, 2011). Igneous intrusions have not been able to date deformation in the KKFTB very precisely (Morley, 2018), but they have been used to constrain the timing of Late Cretaceous-Palaeogene deformation on the Ranong and Khlong Marui Faults (Watkinson et al., 2011), which may have implications for the TPFZ. Apatite fission track ages do not provide information regarding the Indosinian deformation, but have been used to suggest the timing of strike-slip related uplift and exhumation on the Mae Ping Fault zone (Morley et al., 2007). The timing of metamorphism provides some broad constraints on the timing of Indosinian deformation regionally (B), but not in the KKFTB (see review in Morley, 2018). There is Late Cretaceous and Eocene metamorphism that is possibly related to strike-slip or transpressional deformation (see review in Morley, 2012), but the link has not been conclusively demonstrated. Retrograde metamorphism, and syn-kinematic minerals have been dated along the Mae Ping Fault zone, whose timing probably also applies to the TPFZ (Lacassin et al., 1997; Österle et al., 2019). The bottom section 'calcite vein development' shows estimates of relative timing of calcite formation from (Warren et al., 2014). a-d represent different diagenetic cementing events that occurred during

burial, e = structure-related veins formed during Indosinian deformation, f = intrusion related veins, g = veins related to strike-slip deformation, h = veins related to uplift and karst formation. The timing of tectonically-related veins (e,f,g) was based on field observations in 2014. The U-Pb calcite ages in this study demonstrate some overlap, but some differences with the timing of veins (groups e, f and g) from Warren et al. (2014).

Table Captions

Table 1: Sample locations and descriptions

Table 2: LA ICP MS parameters for U-Pb analyses and element mapping

Table 3: Average trace element concentrations for each sample, with standard error of the mean. The concentrations for ^{24}Mg, ^{55}Mn, ^{57}Fe and ^{88}Sr are given in ppm. The other isotopic concentrations are in ppb. The concentrations were obtained from the element maps for each sample. The data for individual spots can be found in Supplementary File 2.

References

Arboit, F., Amrouch, K., Collins, A.S., King, R., Morley, C.K., 2015. Determination of the tectonic evolution from fractures, faults, and calcite twins on the southwestern margin of the Indochina Block. Tectonics 34, 1576-1599.

Arboit, F., Collins, A.S., Morley, C.K., Jourdan, F., King, R., Foden, J., Amrouch, K., 2016a. Geochronological and geochemical studies of mafic and intermediate dykes from the Khao Khwang Fold–Thrust Belt: Implications for petrogenesis and tectonic evolution. Gondwana Research 36, 124-141.

Arboit, F., Collins, A.S., Morley, C.K., King, R., Amrouch, K., 2016b. Detrital zircon analysis of the southwest Indochina terrane, central Thailand: Unravelling the Indosinian orogeny. Geological Society of America Bulletin 128, 1024-1043.

Barber, A.J., Ridd, M.F., Crow, M.J., 2011. The origin, movement and assembly of the pre-Tertiary tectonic units of Thailand, In: Ridd, M.F., Barber, A.J., Crow, M.J. (Eds.), The Geology of Thailand. Geological Society of London, pp. 71-136.

Barker, S.L.L., Cox, S.F., 2011. Oscillatory zoning and trace element incorporation in hydrothermal minerals: insights from calcite growth experiments. Geofluids 11, 48-56.

Beaudoin, N., Lacombe, O., Roberts, N.M.W., Koehn, D., 2018. U-Pb dating of calcite veins reveals complex stress evolution and thrust sequence in the Bighorn Basin, Wyoming, USA. Geology 46, 1015-1018.

Bons, P.D., Elburg, M.A., Gomez-Rivas, E., 2012. A review of the formation of tectonic veins and their microstructures. Journal of Structural Geology 43, 33-62.

Booth, J., Sattayarak, N., 2011. Subsurface Carboniferous – Cretaceous geology of NE Thailand, In: Ridd, M.F., Barber, A.J., Crow, M.J. (Eds.), The Geology of Thailand. Geological Society of London, pp. 184-222.

Burkhard, M., 1993. Calcite twins, their geometry, appearance and significance as stress-strain markers and indicators of tectonic regime: a review. Journal of Structural Geology 15, 351-368.

Cherniak, D.J., 1997. An experimental study of strontium and lead diffusion in calcite, and implications for carbonate diagenesis and metamorphism. Geochimica et Cosmochimica Acta 61, 4173-4179.

Dew, R.E.C., Collins, A.S., Glorie, S., Morley, C.K., Blades, M.L., Nachtergaele, S., King, R., Foden, J., De Grave, J., Kanjanapayont, P., Evans, N.J., Alessio, B.L., Charusiri, P., 2018a.

Probing into Thailand's basement: New insights from U–Pb geochronology, Sr, Sm–Nd, Pb and Lu–Hf isotopic systems from granitoids. Lithos 320-321, 332-354.

Dew, R.E.C., King, R., Collins, A.S., Morley, C.K., Arboit, F., Glorie, S., 2018b. Stratigraphy of deformed Permian carbonate reefs in Saraburi Province, Thailand. Journal of the Geological Society 175, 163-175.

Farkaš, J., Frýda, J., Holmden, C., 2016. Calcium isotope constraints on the marine carbon cycle and CaCO 3 deposition during the late Silurian (Ludfordian) positive δ 13 C excursion. Earth and Planetary Science Letters 451, 31-40.

Ferrill, D.A., Morris, A.P., Evans, M.A., Burkhard, M., Groshong, R.H., Onasch, C.M., 2004. Calcite twin morphology: a low-temperature deformation geothermometer. Journal of Structural Geology 26, 1521-1529.

Frank, J.R., Carpenter, A.B., Oglesby, T.W., 1982. Cathodoluminescence and Composition of Calcite Cement in the Taum Sauk Limestone (Upper Cambrian), Southeast Missouri. 1982 52, 0631-0638.

Gardiner, N.J., Robb, L.J., Morley, C.K., Searle, M.P., Cawood, P.A., Whitehouse, M.J., Kirkland, C.L., Roberts, N.M.W., Myint, T.A., 2016. The tectonic and metallogenic framework of Myanmar: A Tethyan mineral system. Ore Geology Reviews 79, 26-45.

Goodfellow, B.W., Viola, G., Bingen, B., Nuriel, P., Kylander-Clark, A.R.C., 2017. Palaeocene faulting in SE Sweden from U–Pb dating of slickenfibre calcite. Terra Nova 29, 321-328.

Hansberry, R.L., Collins, A.S., King, R.C., Morley, C.K., Giże, A.P., Warren, J., Löhr, S.C., Hall, P.A., 2015. Syn-deformation temperature and fossil fluid pathways along an exhumed detachment zone, khao khwang fold-thrust belt, Thailand. Tectonophysics 655, 73-87.

Hansberry, R.L., King, R., Collins, A.S., Morley, C.K., 2014. Complex structure of an upper-level shale detachment zone: Khao Khwang fold and thrust belt, Central Thailand. Journal of Structural Geology 67, 140-153.

Hansberry, R.L., Zwingmann, H., Loehr, S., Collins, A.S., King, R.C., Morley, C.K., Drysdale, R.N., 2017. Constraining the timing of shale detachment faulting: A geochemical approach. Lithosphere 9, 431-440.

Hansen, B.T., Wemmer, K., 2011. Age and evolution of the basement rocks in Thailand, In: Ridd, M.F., Barber, A.J., Crow, M.J. (Eds.), The Geology of Thailand. Geological Society of London, pp. 19-32.

Hansman, R.J., Albert, R., Gerdes, A., Ring, U., 2018. Absolute ages of multiple generations of brittle structures by U-Pb dating of calcite. Geology 46, 207-210.

Huchon, P., Le Pichon, X., Rangin, C., 1994. Indochina Peninsula and the Collision of India and Eurasia. Geology 22, 27-30.

Lacassin, R., Maluski, H., Leloup, P.H., Tapponnier, P., Hinthong, C., Siribhakdi, K., Chuaviroj, S., Charoenravat, A., 1997. Tertiary diachronic extrusion and deformation of western Indochina: Structural and40Ar/39Ar evidence from NW Thailand. Journal of Geophysical Research: Solid Earth 102, 10013-10037.

Leloup, P.H., Arnaud, N., Lacassin, J.R., Kienast, J.R., Harrison, T.M., Phan Trong, T.T., Replumaz, A., Tapponier, P., 2001. New Constraints on hte Structure, thermichronology, and timing of the Ailao Shan-REd River Shear Zone, SE Asia. Journal of Geophysical Research 106, 6683-6732.

Li, Q., Parrish, R.R., Horstwood, M.S.A., McArthur, J.M., 2014. U–Pb dating of cements in Mesozoic ammonites. Chemical Geology 376, 76-83.

Maskenskaya, O.M., Drake, H., Åström, M.E., 2013. Geochemistry of Calcite Veins: Records of Fluid Mixing and Fluid-Rock Interaction. Procedia Earth and Planetary Science 7, 566-569.

Migdisov, A., Williams-Jones, A.E., Brugger, J., Caporuscio, F.A., 2016. Hydrothermal transport, deposition, and fractionation of the REE: Experimental data and thermodynamic calculations. Chemical Geology 439, 13-42.

Morley, C.K., 2002. A tectonic model for the Tertiary evolution of strike–slip faults and rift basins in SE Asia. Tectonophysics 347, 189-215.

Morley, C.K., 2009. Geometry and evolution of low-angle normal faults (LANF) within a Cenozoic high-angle rift system, Thailand: Implications for sedimentology and the mechanisms of LANF development. Tectonics 28, n/a-n/a.

Morley, C.K., 2012. Late Cretaceous–Early Palaeogene tectonic development of SE Asia. Earth-Science Reviews 115, 37-75.

Morley, C.K., 2018. Understanding Sibumasu in the context of ribbon continents. Gondwana Research 64, 184-215.

Morley, C.K., Ampaiwan, P., Thanudamrong, S., Kuenphan, N., Warren, J., 2013. Development of the Khao Khwang Fold and Thrust Belt: Implications for the geodynamic setting of Thailand and Cambodia during the Indosinian Orogeny. Journal of Asian Earth Sciences 62, 705-719.

Morley, C.K., Charusiri, P., Watkinson, I.M., 2011. Structural geology of Thailand during the Cenozoic, In: Ridd, M.F., Barber, A.J., Crow, M.J. (Eds.), The Geology of Thailand. Geological Society of London, pp. 273-334.

Morley, C.K., Racey, A., 2011. Tertiary stratigraphy, In: Ridd, M.F., Barber, A.J., Crow, M.J. (Eds.), The Geology of Thailand. Geological Society of London, pp. 223-272.

Morley, C.K., Smith, M., Carter, A., Charusiri, P., Chantraprasert, S., 2007. Evolution of deformation styles at a major restraining bend, constraints from cooling histories, Mae Ping fault zone, western Thailand. Geological Society, London, Special Publications 290, 325-349.

Nachtergaele, S., Glorie, S., Morley, C.K., Charusiri, P., Kanjanapayont, P., Vermeesch, P., Carter, A., Van Ranst, G., De Grave, J., 2019. Cenozoic tectonic evolution of southeastern Thailand derived from low-temperature thermochronology. Journal of the Geological Society.

Nantasin, P., Hauzenberger, C., Liu, X., Krenn, K., Dong, Y., Thöni, M., Wathanakul, P., 2012. Occurrence of the high grade Thabsila metamorphic complex within the low grade Three Pagodas shear zone, Kanchanaburi Province, western Thailand: Petrology and geochronology. Journal of Asian Earth Sciences 60, 68-87.

Nazrul, M., 2015. Fluid Evolution Through Different Deformation Stages: A Carbonate Outcrop-Based Study in the Western Highland of Thailand, Department of Geology. Chulalongkorn University, Thailand, p. 39.

Nuriel, P., Weinberger, R., Kylander-Clark, A.R.C., Hacker, B.R., Craddock, J.P., 2017. The onset of the Dead Sea transform based on calcite age-strain analyses. Geology 45, 587-590.

Österle, J.E., Klötzli, U., Stockli, D.F., Palzer-Khomenko, M., Kanjanapayont, P., 2019. New age constraints on the Lan Sang gneiss complex, Thailand, and the timing of activity of the Mae Ping shear zone from in-situ and depth-profile zircon and monazite U-Th-Pb geochronology. Journal of Asian Earth Sciences 181.

Palin, R.M., Searle, M.P., Morley, C.K., Charusiri, P., Horstwood, M.S.A., Roberts, N.M.W., 2013. Timing of metamorphism of the Lansang gneiss and implications for left-lateral motion along the Mae Ping (Wang Chao) strike-slip fault, Thailand. Journal of Asian Earth Sciences 76, 120-136.

Paquette, J., Reeder, R.J., 1995. Relationship between surface structure, growth mechanism, and trace element incorporation in calcite. Geochimica et Cosmochimica Acta 59, 735-749.

Parrish, R.R., Parrish, C.M., Lasalle, S., 2018. Vein calcite dating reveals Pyrenean orogen as cause of Paleogene deformation in southern England. Journal of the Geological Society 175, 425-442.

Paton, C., Hellstrom, J., Paul, B., Woodhead, J., Hergt, J., 2011. Iolite: Freeware for the visualisation and processing of mass spectrometric data. Journal of Analytical Atomic Spectrometry 26.

Petrus, J.A., Chew, D.M., Leybourne, M.I., Kamber, B.S., 2017. A new approach to laser-ablation inductively-coupled-plasma mass-spectrometry (LA-ICP-MS) using the flexible map interrogation tool ‘Monocle’. Chemical Geology 463, 76-93.

Reeder, R.J., Fagioli, R.O., Meyers, W.J., 1990. Oscillatory Zoning of Mn in Solution-grown Calcite Crystals. Earth-Science Reviews 29, 39-46.

Rhodes, B.P., Charusiri, P., Kosuwan, S., Lamjuan, A., 2005. Tertiary Evolution of the Three Pagodas Fault, Western Thailand, Proceedings of the International Conference on Geology, Geotechnology and Mineral Resources of Indochina, Khon Kaen, Thialand., pp. 498-505.

Ridd, M.F., Barber, A.J., Crow, M.J., 2011. Introduction to the geology of Thailand, In: Ridd, M.F., Barber, A.J., Crow, M.J. (Eds.), The Geology of Thailand. Geological Society of London, pp. 1-18.

Roberts, N.M.W., 2018. Progress in Crustal deformation and fluid-flow using U-Pb carbonate geochronology, 15th International Conference on Gondwana to Asia IAGR, Xian, China, pp. 69-70.

Roberts, N.M.W., Drost, K., Horstwood, M.S.A., Condon, D.J., Chew, D., Drake, H., Milodowski, A.E., McLean, N.M., Smye, A.J., Walker, R.J., Haslam, R., Hodson, K., Imber, J., Beaudoin, N., Lee, J.K., 2020. Laser ablation inductively coupled plasma mass spectrometry (LA-ICP-MS) U-Pb carbonate geochronology: strategies, progress, and limitations. Geochronology 2, 33-61.

Roberts, N.M.W., Rasbury, E.T., Parrish, R.R., Smith, C.J., Horstwood, M.S.A., Condon, D.J., 2017. A calcite reference material for LA-ICP-MS U-Pb geochronology. Geochemistry, Geophysics, Geosystems 18, 2807-2814.

Roberts, N.M.W., Walker, R.J., 2016. U-Pb geochronology of calcite-mineralized faults: Absolute timing of rift-related fault events on the northeast Atlantic margin. Geology 44, 531-534.

Searle, M.P., Morley, C.K., 2011. Tectonic and thermal evolution of Thailand in the regional context of SE Asia, In: Ridd, M.F., Barber, A.J., Crow, M.J. (Eds.), The Geology of Thailand. Geological Society of London, pp. 539-572.

Sone, M., Metcalfe, I., 2008. Parallel Tethyan sutures in mainland Southeast Asia: New insights for Palaeo-Tethys closure and implications for the Indosinian orogeny. Comptes Rendus Geoscience 340, 166-179.

Stacey, J.S., Kramers, J.D., 1975. Approximation of terrestrial lead isotope evolution by a two-stage model. Earth and Planetary Science Letters 26, 207-221.

Ueno, K., Charoentitirat, T., 2011. Carboniferous and Permian, In: Ridd, M.F., Barber, A.J., Crow, M.J. (Eds.), The Geology of Thailand. Geological Society of London, p. 0.

Ueno, K., Miyahigashi, A., Charoentitirat, T., 2010. The Lopingian (Late Permian) of mid-oceanic carbonates in the Eastern Palaeotethys: stratigraphical outline and foraminiferal faunal succession. Geological Journal 45, 285-307.

Upton, D.R., 1999. A Regional Fission Track Study of Thailand: Implications for Thernal Histroy and Denudation. Birkbeck (University of London), University of London Thesis, p. 784.

Vermeesch, P., 2018. IsoplotR: A free and open toolbox for geochronology. Geoscience Frontiers 9, 1479-1493.

Warren, J., Morley, C.K., Charoentitirat, T., Cartwright, I., Ampaiwan, P., Khositchaisri, P., Mirzaloo, M., Yingyuen, J., 2014. Structural and fluid evolution of Saraburi Group sedimentary carbonates, central Thailand: A tectonically driven fluid system. Marine and Petroleum Geology 55, 100-121.

Watkinson, I., Elders, C., Batt, G., Jourdan, F., Hall, R., McNaughton, N.J., 2011. The timing of strike-slip shear along the Ranong and Khlong Marui faults, Thailand. Journal of Geophysical Research: Solid Earth 116.

Sample	Coordinates	Description (see figures 3 - 6)
Khao Khwang Fold and Thrust belt (KKFTB)		
7b	14°42.266'N, 100°53.122'E	Sampled from an out of sequence thrust zone in a fault-propagation-fold. Deformation is hypothesised to be Indosinian in age.
8b	14°42.783'N, 100.52.250'E	Sampled from an over-pressured \`explosion\` brecciated limestone. Hypothesised to be Cenozoic in age.
10b	14°36.554'N, 101°23.478'E	Sampled from a folded vein, associated with flexural slip. Hypothesised to be Indosinian stage II in age.
Three Pagodas Fault zone (TPFZ)		
12a	14°14.011'N, 99°14.303'E	Sampled in a road cutting on highway 3199 (near Chong Sadao). Sample from a fault breccia formed from hydrofracturing. Hypothesised to be Cenozoic in age.

Table 1. Sample locations and descriptions

Laser	
Brand and Model	RESOlution-LR 193nm Excimer Laser System
Wavelength	193nm
Pulse Duration	20ns
Spot Size (U-Pb analysis)	110µm, (75µm - NIST614)
Spot Size (Elemental mapping)	91x91 (75µm NIST612)
Repetition Rate	10Hz
Energy Attenuation	100%T (50% NIST612)
Laser Fluency	8 j/cm^2
ICPMS	
Brand and Model	Agilent 7900x
Forward Power	1350W
Torch Depth	4.5mm
Gas Flows	
Plasma (Ar) **Auxiliary (Ar)**	15L/min 1L/min
Carrier (He)	07L/min
Sample (Ar)	0.88L/min
Data Acquisition Parameters	
Data Acquisition Protocol	Time resolved analysis
Scanned Isotopes (U-Pb analysis)	43Ca, 202Hg 204Pb, 206Pb, 207Pb, 208Pb, 232Th 238U
Scanned Isotopes (elemental mapping)	24Mg, 27Al, 29Si, 43Ca, 55Mn, 56Fe, 88Sr, 130Ba, 139La, 140Ce, 141Pr, 146Nd, 147Sm, 153Eu, 157Gd, 159Tb, 163Dy, 165Ho, 166Er, 169Tm, 172Yb, 175Lu, 202Hg, 204Pb, 206Pb, 207Pb, 208Pb, 232Th, 238U
Detector Mode	Peak Hopping, Pulse & Analog counting
Background Collection	30s (spot analysis) 10s (mapping)
Ablation for Age Calculation	30s (ablation time for mapping varied by line length)
Washout	20
Standards	
Primary Standards (U-Pb analysis)	NIST614
Secondary Standards (U-Pb analysis)	WC-1, ‘Prague’
Primary Standards (elemental mapping)	NIST612

Table 2: LA ICP MS parameters for U-Pb analyses and element mapping

Sample	ppm ^{24}Mg	^{55}Mn	^{57}Fe	^{88}Sr	ppb ^{137}Ba	^{139}La	^{140}Ce	^{141}Pr	^{146}Nd	^{147}Sm	^{153}Eu	^{157}Gd	^{159}Tb	^{163}Dy	^{165}Ho	^{166}Er	^{169}Tm	^{172}Yb	^{175}Lu	^{206}Pb	^{207}Pb	^{208}Pb	^{232}Th	^{238}U
8b	2348	120	413	1085	386	119	124	24	134	35	18	43	4.9	25	4.9	10	1.0	4.8	0.4	43	33	31	2.5	272
	75	4	14	60	32	29	23	4	23	6	3	6	1.0	4	1.0	2	0.3	1.5	0.2	8	7	7	1.4	62
12a	5800	26	33	509	1226	1362	2550	303	1207	231	43	225	34	219	44	119	15	91	12	120	82	84	9.3	718
	757	1	1	12	87	140	265	31	113	18	4	14	2	13	3	8	1	8	1	86	60	60	0.8	168
10b	2154	11	66	1997	3432	896	433	126	595	112	19	163	21	142	33	92	10	54	7.7	210	112	111	1.2	528
	321	1	1	265	835	288	132	38	183	36	6	51	7	44	10	28	3	16	2.3	62	46	46	0.3	61
7b	3709	27	595	494	440	629	412	97	504	130	32	178	23	153	36	102	11	54	7.9	58	20	25	2.2	347
	385	2	60	39	56	101	70	18	102	33	10	54	7	51	13	35	4	22	3.3	7	2	2	0.6	28

Highlights

- First calcite U-Pb geochronlogy on tectonic veins in Thailand
- Timing of calcite precipitation is constrained to Indosinian II and Cenozoic
- Redox-sensitive element maps are used to decipher U-Pb data

CRediT author statement

Alexander Simpson: method development, data collection, manuscript drafting. **Stijn Glorie:** conceptualization, fieldwork, method development, manuscript reworking, supervision. **Chris Morley:** conceptualization, geological setting, manuscript reviewing. **Nick Roberts:** methodology, manuscript reviewing. **Jack Gillespie:** methodology, manuscript reviewing. **Jack Lee:** data collection